Optics & Laser Technology 141 (2021) 107102

Contents lists available at ScienceDirect

Optics and Laser Technology

journal homepage: www.elsevier.com/locate/optlastec

Full length article

Towards remotely directional transmission of terahertz wave in air: The concept of free-space photonic crystal waveguide

Lie-Zhi Tang [a], Jia-Yu Zhao [a,b,*], Zhang-Hua Dong [a], Zhong-Hui Liu [a], Wen-Ting Xiong [a], Yu-Chen Hui [a], Alexander Shkurinov [c], Yan Peng [a,b], Yi-Ming Zhu [a,b]

[a] Terahertz Technology Innovation Research Institute, Terahertz Spectrum and Imaging Technology Cooperative Innovation Center, Shanghai Key Lab of Modern Optical System, University of Shanghai for Science and Technology, Shanghai 200093, China

[b] Shanghai Institute of Intelligent Science and Technology, Tongji University, Shanghai 200092, China

[c] Faculty of Physics and International Laser Center, Lomonosov Moscow State University, Moscow 119991, Russia

ARTICLE INFO

Keywords:
Hollow cylindrical plasma waveguide
Free-space photonic crystal
Terahertz waveguide
Attenuation length
Single-mode property

ABSTRACT

Remotely directional transmission of terahertz (THz) wave in free space is essential in fields of astronomy, space and ground based communications, as well as sensing for atmospheric pollutants, etc. In previous studies, large-aperture halfway mirrors were employed in order to fully collect and then focus the heavily naturally diffracted beam of THz wave to the final target. In this case, however, the broad THz beam not only made a large-size transmission system, but also led to a heavy energy loss due to water vapor absorption within the beam cross-section. Here, we theoretically proposed two index-guiding-based THz waveguide structures composed of plasma filament arrays in air, i.e., hollow cylindrical plasma (HCP) waveguide and free-space photonic crystal (FPC) waveguide (triangular lattice point matrix with a central point defect). Both structures have been demonstrated to well support THz propagation modes, which were confined inside the tiny central air core of the waveguide for an attenuation length up to hundreds of meters. Compared with each other, the FPC waveguide exhibited better performances, including smaller mode field diameter, longer attenuation length and better single-mode property for a broad THz band, making this scheme a promising candidate for long-distance guidance of THz waves in the atmosphere.

1. Introduction

Long-range directional transmission of terahertz (THz) wave is significantly important for many applications such as astronomy [1,2], space and ground based communications [3,4], as well as remote sensing [5,6]. Recently, 910-m free-space propagation of THz pulses through the atmosphere has been realized [7,8]. This achievement relied not only on the high THz intensity radiated from the large-aperture photo-conductive antenna (PCA) which overcame the water vapor absorption loss in the transmission path, but also on the large diameter of the halfway mirror (~1 m) that collected and then collimated (or loosely focused) the heavily diffracted THz beam towards the target (detection setup).

In this situation, however, the strong natural diffraction of the THz beam would inevitably increase the size of the whole transmission system since large-aperture optical elements have to be set in the beam path. What's worse, the THz energy attenuation caused by the water vapor absorption is obviously greater within a larger cross-section of the diffracted THz beam than a narrower beam case. These issues are major obstacles to expedite the application of THz technology in the atmosphere.

One may wonder that if the diameter of the THz beam could be compressed (better into the scale of its wavelength) for a long distance, both of the aforementioned problems are expected to be solved at the same time. Moreover, the lost high-frequency THz spectral components (greater than 0.4 THz) in the literature [8] might also be retrieved, meeting the urgent demand for the next generation of communications towards high & broad frequency band.

Hence, in recent years, THz waveguides have attracted extensive attention, including metal circular waveguide [9], parallel plane metal waveguide [10,11], polymer waveguide [12], wire waveguide [13], and photonic crystal fiber [14], etc. Nevertheless, these waveguides, clearly,

* Corresponding author at: Terahertz Technology Innovation Research Institute, Terahertz Spectrum and Imaging Technology Cooperative Innovation Center, Shanghai Key Lab of Modern Optical System, University of Shanghai for Science and Technology, Shanghai 200093, China.

E-mail address: zhaojiayu@usst.edu.cn (J.-Y. Zhao).

https://doi.org/10.1016/j.optlastec.2021.107102
Received 15 August 2020; Received in revised form 24 February 2021; Accepted 19 March 2021
0030-3992/© 2021 Elsevier Ltd. All rights reserved.

cannot be practically applied in directional THz beam transmission systems in free space aiming at communications or remote sensing.

Another promising candidate for guiding THz wave is the femtosecond laser filament [15], which is known as a unique nonlinear optical phenomenon being able to generate a long air-plasma channel up to hundreds or even thousands of meters [16–18], around the focus of a femtosecond laser beam in air. It has been reported that a filament-array based hollow cylindrical plasma (HCP) waveguide, formed by positioning a large number of parallel filaments in a thick ring as the cladding (as shown in Fig. 1(a,d)), could constrain and guide microwave [19,20], infrared [21] and even visible light [22] inside its central tiny air core, resulting in a low transmission loss. The underlying mechanism can be roughly summarized as the fact that the plasma cladding acts as mirrors to the confined electromagnetic (EM) waves when its plasma density is larger than the critical $N_{cr} = \varepsilon_0 m_e \omega_{EM}^2 / e^2$ [20].

Inspired by the above works mainly in microwave band, in the current paper, affords have been made on both analytical and numerical investigations of filament-array based THz waveguide. It has been revealed that a HCP waveguide can successfully achieve a long-distance (a few hundred meters) transmission of THz wave with low attenuation. Specifically, two THz propagation modes, namely, TE_{01} and TE_{11}, were studied. And the former has been proved to be with much longer attenuation length, especially towards high THz band. Note that, here the attenuation length is defined as the inverse of the imaginary part of a modal propagation constant.

More importantly, the spatial locations of plasma filaments in the array can be flexibly controlled, either by modulating the planar distribution of the laser energy with a phase plate [23], or by adjusting the focusing lens array [24] within the cross-section of the laser beam. This is the most unique aspect for a filament-array based THz waveguide to be different from a traditional one [9–14].

Thus, in this work, we re-arranged the HCP array into a triangular lattice point matrix with a central point defect, i.e., a free-space photonic-crystal-like (FPC) structure (as shown in Fig. 1(e,f)). In this way, much less (36) filaments were used, instead of hundreds (Fig. 1(a,b)) or even thousands [25] to be needed. It has been demonstrated that under the same situation of 36 standard filaments (plasma density $N_e \sim 10^{17}$ cm^{-3}) being adopted, the FPC structure exhibits better performances, including smaller mode field diameter, longer attenuation length (i.e., lower transmission loss), and better single-mode property, all for a wide band ranging from 1 to 10 THz, as well as a low dispersion towards high THz band. Therefore, it is more efficient to apply a plasma based FPC structure as the THz waveguide than the HCP scheme in both views of laser energy saving and THz wave transmission effects.

2. The hollow cylindrical plasma (HCP) waveguide

2.1. The HCP structure

The HCP array is built by a set of laser plasma filaments generated by

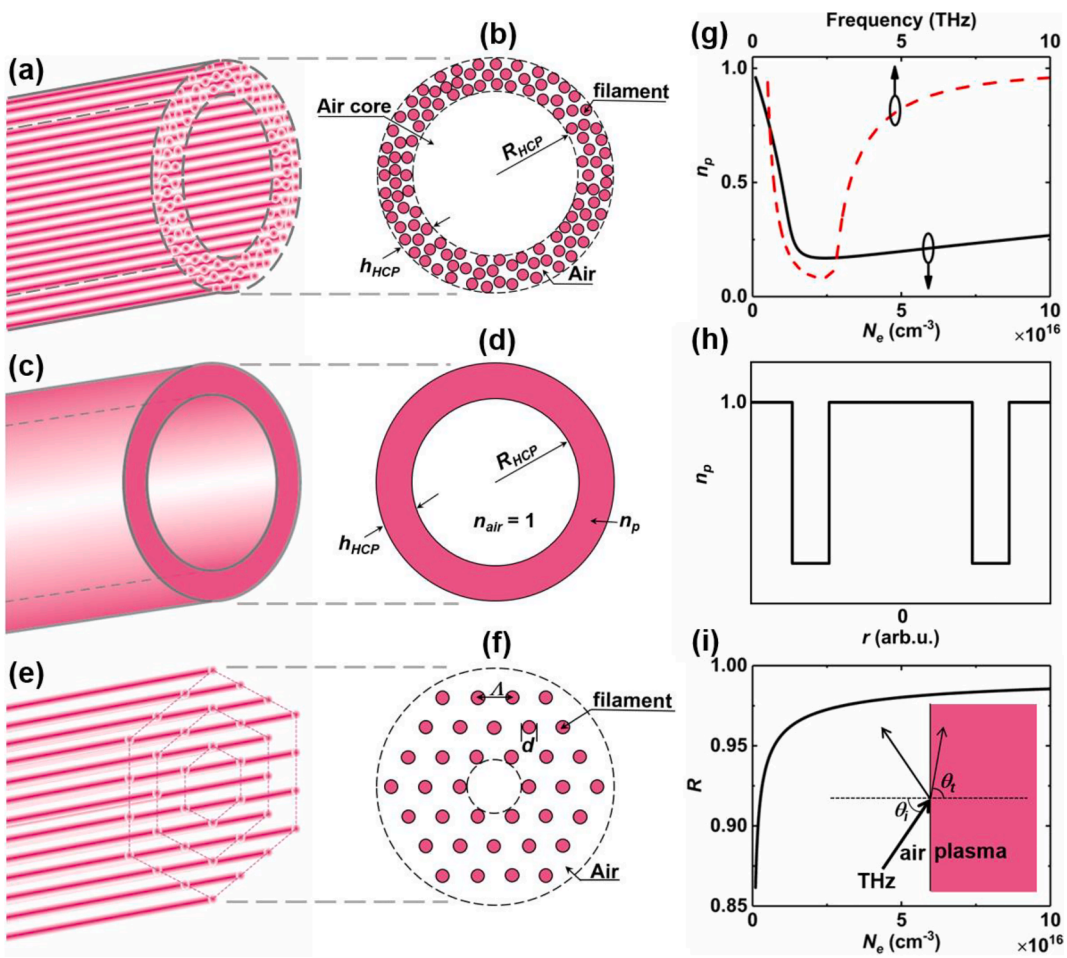

Fig. 1. Side and transverse views of (a,b) the hollow cylindrical plasma (HCP) array and (c,d) its simplified distributions, as well as (e,f) the free-space photonic crystal (FPC) structure. R_{HCP} is the inner radius of the HCP waveguide; h_{HCP} and n_p are the thickness and the refractive index of the HCP cladding, respectively; Λ is the lattice constant and d is the diameter of a single plasma filament. (g) The plasma refractive index n_p as functions of THz frequency (at $N_e = 10^{17}$ cm^{-3}) and plasma density N_e (at $f = 1$ THz). (h) The radial n_p distribution of the HCP waveguide. (i) THz reflectivity R as a function of N_e, in case of $\lambda = 300$ μm (1 THz) and $R_{HCP} = 1300$ μm. Inset: θ_i and θ_t represent the angles of the incident and refracted THz rays on the air-plasma interface.

the propagation of femtosecond laser pulses in the air, as shown in Fig. 1 (a). The structure's cladding consists of a large number of randomly densely arranged plasma filaments with an average spacing between each other smaller than the THz wavelength, as shown in Fig. 1(b). In practice, such a plasma channel can be produced by using an appropriate set of phase masks or deformable mirrors to partition or regularize the laser beam [23,24], which is similar to that used by Chateauneuf *et al.* [25]. This initial intensity modulation will initiate the origin of the filaments in the plane of the pulse cross-section despite of random fluctuation, which achieves the stabilization of the parameters of the plasma channel [26]. In order to facilitate the following analyses and calculations, the HCP structure in Fig. 1(a,b) has been simplified into a thick ring with homogeneous plasma density as shown in Fig. 1(c,d).

2.1.1. W-type Radial refractive index distribution of the HCP waveguide

The radial refractive index distribution of the HCP waveguide can be quantified by calculating the refractive index of the plasma cladding [27,28]:

$$\overline{n_p} = n_p + iK_p = \sqrt{1 + \frac{\omega_p^2}{i\omega\nu - \omega^2}} \tag{1}$$

where n_p and K_p are real and imaginary parts of $\overline{n_p}$, respectively; $\nu \sim 1$ THz corresponds to the typical electron collision frequency inside the filament [29]. ω is the THz frequency and ω_p indicates the plasma frequency (in SI units) [27,28]:

$$\omega_p = \sqrt{N_e e^2/m_e\varepsilon_0} \tag{2}$$

where e and m_e are the charge and mass of an electron, respectively, and ε_0 is the vacuum permittivity. N_e denotes the number density of electrons, between 10^{15} and 10^{17} cm^{-3} [30].

By calculating Eq. (1–2), n_p can be obtained as functions of f and N_e, as plotted in Fig. 1(g). One can see that n_p is basically less than the unity when $f = 0.5$ to 10 THz or $N_e = 10^{15}$ to 10^{17} cm^{-3}. The corresponding radial n_p distribution of the HCP waveguide (Fig. 1(d)) is schematically shown in Fig. 1(h). It can be seen that the refractive index of the plasma cladding is less than that of the air core and surroundings (~1), making the whole profile similar to the reported W-type fiber with tight confinement and low absorption loss for 1.55-μm light [31,32]. In Section 2.2, the validity of our W-type n_p distribution (Fig. 1(h)) on THz wave transmission will be analytically verified. Moreover, in Section 2.3, numerical simulations of THz waveguiding based on this refractive index distribution are also performed.

2.1.2. High THz reflectivity inside the air core of the HCP waveguide

The guidance of THz wave via the HCP waveguide is crucially related to the magnitude of THz reflectivity on the inner face of the plasma cladding. The reflection coefficient R (differ from R_{HCP}) is given by [19]:

$$R = \left|\frac{cos\theta_i - n_p cos\theta_t}{cos\theta_i + n_p cos\theta_t}\right|^2 \tag{3}$$

where θ_i and θ_t are THz incidence and refraction angles, respectively, following the Snell's law:

$$n_{air} sin\theta_i = n_p sin\theta_t \tag{4}$$

This relationship is further displayed as inset in Fig. 1(i). Furthermore, considering the diffraction propagation of THz wave inside the central air core with radius of R_{HCP}, the diffraction angle at the incident port of the waveguide is $\phi \approx \sin^{-1}(\lambda/2R_{HCP})$ [19,20]. Then, the incident angle of the THz wave on the inner face of the plasma cladding is $\theta_i = \pi/2 - \phi = \pi/2 - \sin^{-1}(\lambda/2R_{HCP})$, which is only associated with λ and R_{HCP}. Meanwhile, θ_t can be determined by Eq. (4) with a certain θ_i.

Next, by solving Eqs. (3) and (4), the THz reflection coefficient R with respect to N_e was obtained, as shown in Fig. 1(i). It is clear that the increasing N_e leads to a higher THz reflectivity when λ is fixed at 300 μm (1 THz) and R_{HCP} is set to be 1300 μm. And R exceeds 98% when N_e reaches 4.85×10^{16} cm^{-3}. This further indicates that the suggested HCP waveguide structure can indeed play the role of a plasma mirror [33] before realizing THz mode guiding.

2.1.3. Determining the cladding thickness of the HCP waveguide

The calculated high THz reflectivity in the previous section, however, cannot completely avoid the penetration of THz energy into the plasma cladding or even into the ambient air. Hence, in order to suppress the possible THz mode leaking, the plasma cladding needs to be enhanced in thickness to reduce the field of the permeable THz wave. In other words, h_{HCP} (Fig. 1(d)) should exceed the skin depth δ of the THz field inside the plasma, which can be calculated as [19]:

$$\delta = \sqrt{2/\sigma_p\omega_{THz}\mu_0} \tag{5}$$

where μ_0 is the permeability of free space and $\sigma_p = \omega_p^2\varepsilon_0\nu/(\omega_{THz}^2 + \nu^2)$ is the plasma conductivity [28].

By calculating Eq. (5) in THz band, δ is found to be generally greater than the diameter of a single filament (~100 μm). For example: δ is between 103 and 177 μm in case of $f = 3.35$ to 10 THz at $N_e = 10^{17}$ cm^{-3}. When $N_e = 10^{15}$ or 10^{16} cm^{-3}, δ is larger than 100 μm for the entire THz band (0.1 ~ 10 THz) with the minimum of 113.56 μm and maximum of 1800 μm. In order to fulfill the condition of $h_{HCP} > \delta$, the HCP waveguide cladding needs to be built by multi-layer plasma filaments, e.g., as shown in Fig. 1(a,b).

2.2. Analytical model of the HCP waveguide

In this section, analytical models have been applied aiming at quantitatively revealing the transmission properties of THz wave inside the HCP waveguide.

2.2.1. Attenuation length of the transmission mode

Here, we study the possible THz transmission modes inside the HCP waveguide by solving the corresponding propagation constant, which is derived from the characteristic equation and decided by the boundary conditions. In view of the HCP waveguide structure established in Fig. 1 (c,d), we can get the simplified characteristic equation for the lowest loss mode TE_{0m} [19]:

$$\frac{1}{u}\frac{J_1(u)}{J_0(u)} = \frac{1}{w}\frac{H_1^{(1)}(w)}{H_0^{(1)}(w)} \tag{6}$$

where $u = R_{HCP}(k_0^2 - h^2)^{1/2}$, $w = R_{HCP}(k_p^2 - h^2)^{1/2}$ are the normalized transverse phase parameters and normalized transverse attenuation parameters, respectively; $h = h' + ih''$ is the mode propagation constant, where the real part h' determines the phase velocity and the imaginary part h'' describes the loss; $k_0 = \omega_{THz}(\mu_0\varepsilon_0)^{1/2}$ is the wavenumber inside the HCP waveguide; $k_p = (\omega_{THz}\mu_p\sigma_p)^{1/2}\exp(j\pi/4)$ is the wavenumber inside the plasma cladding; J_n and $H_n^{(1)}$ are the n order Bessel functions of the first kind and the n order Hankel functions of the first kind, respectively.

Eq. (6) usually has several roots corresponding to various transverse axisymmetric modes. The maximum propagation distance corresponds to the lowest transverse mode TE_{01}. Each mode has a cut-off wavelength which is determined by the value of u when $w = 0$, and u is referred to as the cut-off normalized transverse phase parameters, i.e., $u_{c01} = 3.832$, which is the first root of the Bessel function $J_1(u) = 0$. Similarly, the fundamental transmission mode TE_{11} with the lowest cut-off frequency can also be obtained by simplifying the characteristic equation [34]. For TE_{11}, the cut-off normalized transverse phase parameters is $u_{c11} = 1.84$, which is the root of the first order Bessel functions derivative.

The critical wave vector k_{cut} ($k_{cut} = 2\pi/\lambda_{cut} = u_c/R_{HCP}$) determines the upper limit of THz radiation. The related geometric parameters of the

HCP waveguide operating in TE_{01} and TE_{11} modes can be obtained as follows [19,34]:

$$\begin{aligned} TE_{01} &: \lambda_{THz} < \lambda_{cut01} = 2\pi/_{k_{cut01}} = 1.64R_{HCP} \\ TE_{11} &: \lambda_{THz} < \lambda_{cut11} = 2\pi/_{k_{cut11}} = 3.4R_{HCP} \end{aligned} \tag{7}$$

One can numerically solve h of TE_{01} and TE_{11} by Eq. (7), and the results are [34,35]:

$$\begin{aligned} TE_{01} &: h'' \approx u_{c01}^2 \Bigg/ \left(k_0^2 R_{HCP}^3 \sqrt{\frac{2\omega_p^2}{\nu\omega_{THz}}} \right) \\ TE_{11} &: h'' = \frac{\delta\left(k_0^2 + u_{c11}^2\left(u_{c11}^2 - 1\right)/R_{HCP}^2\right)}{2\left(u_{c11}^2 - 1\right)R_{HCP}\sqrt{k_0^2 - \left(u_{c11}/R_{HCP}\right)^2}} \end{aligned} \tag{8}$$

At last, the attenuation lengths ($1/h''$) of TE_{01} and TE_{11} were obtained dependent on f and shown in Fig. 2(a) as the dash black line and the solid red line, respectively.

In Fig. 2(a), it can be seen that for TE_{11} mode, $1/h''$ basically decreases with the increasing frequency in the whole THz band, and the maximum value is about 0.035 m at 0.15 THz. In contrast, $1/h''$ of TE_{01} mode exhibits quite a different variation trend, which increases towards high THz band without becoming obviously saturated, overall much larger than that of TE_{11} mode. This might be due to the larger mode field distribution of TE_{11} (please see Section 2.3), which would penetrate more strongly into the nearby inner cladding of the HCP waveguide [36]. Nevertheless, as the frequency increases, the TE_{01} mode electric field tends to shrink inside the core area of the HCP waveguide [37], resulting in an increasing attenuation length.

Since TE_{01} is the main transmission mode along the proposed HCP waveguide structure, next, detailed analyses were carried out on the TE_{01} mode, including the influences of R_{HCP} and N_e on its attenuation length $1/h''$, as well as its radial mode field distribution feature.

2.2.2. The modal properties of TE_{01}

Firstly, $1/h''$ of TE_{01} mode at different R_{HCP} was calculated according to Eq. (8) and results are shown in Fig. 2(b,c). Fig. 2(b) shows that in the whole THz band, the overall $1/h''$ increases with R_{HCP} at a fixed $N_e = 10^{17}$ cm^{-3}, which means that the HCP waveguide with larger R_{HCP} suffers from less transmission loss. This point can be interpreted by the fact that larger R_{HCP} results in larger θ_i given by $\theta_i = \pi/2 - \sin^{-1}(\lambda/2R_{HCP})$, i.e., the THz wave propagates more parallel to the air-plasma interface. Therefore, there are not only less number of THz reflections along the same waveguide but also higher reflectivity R for each internal reflection. As a result, the transmission loss decreases. On the other hand, one can increase N_e in order to obtain a larger $1/h''$. Fig. 2(c) shows a positive correlation relationship between $1/h''$ and N_e at $f = 1$ THz, which agrees with Fig. 1(i) since a larger N_e leads to a higher R of the THz wave inside the waveguide air core.

Secondly, as for the mode field distribution of TE_{01} inside the HCP waveguide, it is considered to be deduced by using the weak guiding approximation which is defined as [19]:

$$H_r = \begin{cases} -j\dfrac{h}{k_1}AJ_1(k_1 r) & r < R_{HCP} \\ j\dfrac{h}{k_2}BH_1^{(1)}(k_2 r) & R_{HCP} < r < R_{HCP} + h_{HCP} \\ CK_0(k_1 r) & r > R_{HCP} + h_{HCP} \end{cases} \tag{9}$$

where A, B and C are the field amplitude coefficients; K_0 is the zero order

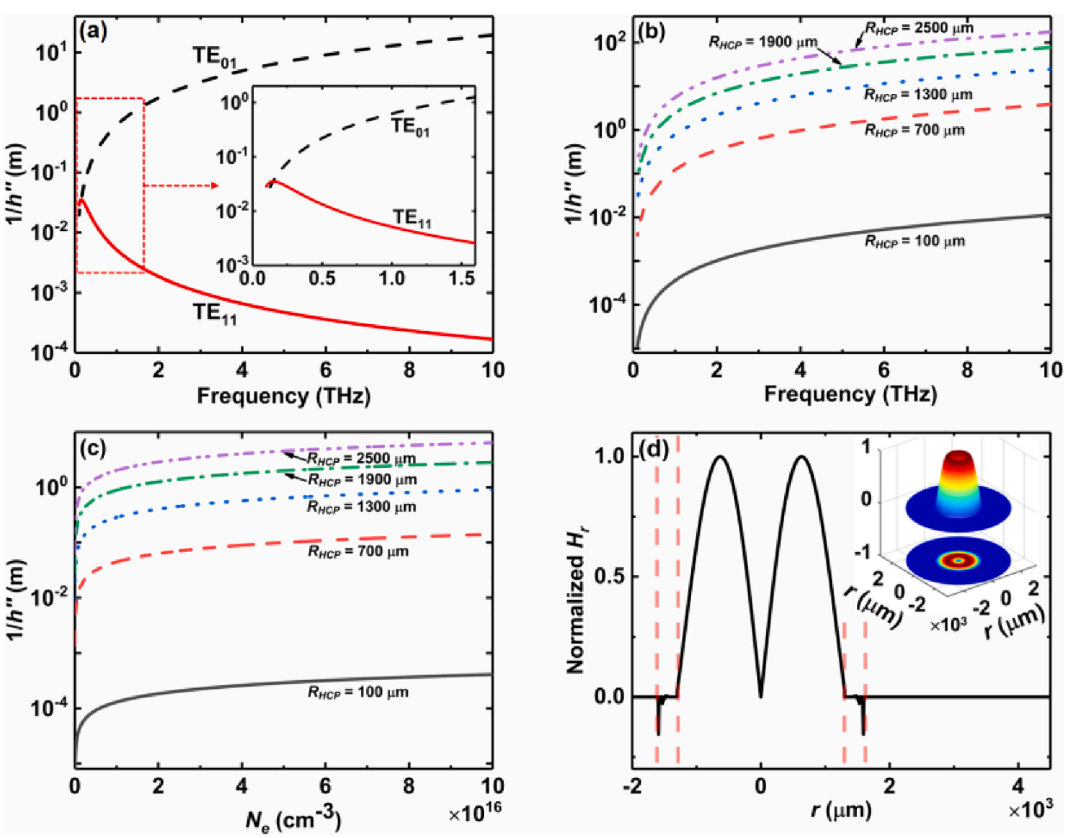

Fig. 2. (a) Attenuation lengths $1/h''$ of TE_{01} and TE_{11} as a function of frequency f for $N_e = 10^{17}$ cm^{-3} and $R_{HCP} = 1300$ μm. Inset: enlarged detail from $f = 0$ to 1.6 THz. $1/h''$ of TE_{01} as a function of (b) f (with $N_e = 10^{17}$ cm^{-3}) and (c) N_e (at $f = 1$ THz) at different R_{HCP}. (d) The radial mode field distribution of TE_{01} inside the HCP waveguide (the red dashed lines highlight the waveguide cladding). Inset: field intensity distribution obtained by rotating the normalized H_r curve around the axis of $r = 0$ μm.

virtual argument Bessel functions of the second kind and $k_1 = (k_0^2 - h^2)^{1/2}$, $k_2 = (k_p^2 - h^2)^{1/2}$. Based on Eq. (9), TE_{01} mode field H_r inside the HCP waveguide has been calculated and shown in Fig. 2(d) at $f = 0.5$ THz, $N_e = 10^{17}$ cm^{-3}, $R_{HCP} = 1300$ μm, $h_{HCP} = 300$ μm, and $r \in$ [-3000, 3000 μm]. It can be seen that the TE_{01} mode field presents in a ring shape, and drastically decreases to zero at the interface between the air core and inner cladding. In addition, the inset in Fig. 2(d) is the schematic diagram of 2-D modal distribution of TE_{01} obtained by rotating the normalized H_r curve once around the axis of $r = 0$ μm. In the next section, numerical simulations will verify this annular mode field distribution inside the HCP waveguide.

2.3. Numerical model of the HCP waveguide

It has been proved that the HCP waveguide can transmit THz wave along the filament array for a long distance, according to the above analytical calculations. However, the corresponding solution procedure is relatively complex. For example, h can only be obtained when the characteristic equation is solved while it is difficult to decide the value of u ($u = R_{HCP}(k_0^2 - h^2)^{1/2}$), because the characteristic equation is transcendental.

Thus in this section, the numerical simulation method has been suggested since it can quickly predict the transmission characteristics of THz wave inside the HCP waveguide. Here, COMSOL Multiphysics, a commercial software equipped with the full-vector finite-element method (FEM) was adopted to simulate the THz mode field and attenuation length in the same HCP waveguide as Section 2.2. The THz refractive index distribution in Fig. 1(h) was pre-configured in the FEM model, as shown in Fig. 3(a), in which parameters of the HCP waveguide were also marked. It is worth mentioning that, the perfect matching layer (PML) was set in order to reduce the reflected wave to a very low level and increase the accuracy of simulations. Parameter values for numerical simulations are listed in Table 1. The fact that h_{HCP} needs to be greater than δ (calculated by N_e and f) has also been taken into consideration.

Then, possible THz mode field distributions inside the transverse cross-section of the HCP waveguide were numerically simulated. Two representative outcomes, i.e., TE_{01} and TE_{11} modes obtained at $N_e = 10^{17}$ cm^{-3} and $f = 0.2$ THz are shown in Fig. 3(b) and (c), respectively,

Table 1
Simulation parameters of the HCP waveguide with three different N_e.

N_e (cm^{-3})	10^{15}	10^{17}	10^{19}
f (THz)		0.1–2	
δ (μm)	359–822	36–80	3.48–8.85
R_{HCP} (μm)	1300		
h_{HCP} (μm)	1500	300	100
L_{PML} (μm)	200		
L_{air} (μm)	1700		

with color (z-component of the Poynting vector) and black arrows (electric field vector). Notably, the ring-shape profile of the TE_{01} mode field is consistent with the calculated result as shown in Fig. 2(d), and the modal distribution area of TE_{11} is larger as expected.

Meanwhile, the attenuation lengths for TE_{01} and TE_{11} modes at different N_e and f have also been obtained during COMSOL simulations and are displayed in Fig. 3(d-f), respectively. It can be seen that the attenuation length of TE_{01} increases with the growth of f, overall larger than that of TE_{11} whose variation trend is first rise and then fall. These observations are basically consistent with the analytic results as shown in the inset of Fig. 2(a). Moreover, it is worth mentioning the following two aspects:

Firstly, the absences of some attenuation length values for TE_{11} towards high frequency in Fig. 3(d,e) might be due to its conversion into the low-loss hybrid mode HE_{11} for stable transmission [38,39]. When N_e is large enough, e.g. in Fig. 3(f), high reflectivity R of the plasma cladding could then maintain the existence of TE_{11} mode within the whole f region being considered.

Secondly, one may also notice the quantitative difference between attenuation lengths of TE_{01} (or TE_{11}) in Fig. 2(a) and 3(e) achieved in the same situation of $N_e = 10^{17}$ cm^{-3}. This could be attributed to the fact that the analytical calculation formula does not involve h_{HCP} of the HCP cladding, which however must be set in the numerical models.

3. Free-space photonic-crystal-like (FPC) structure

According to the above sections, it can be seen that the HCP array could make an effective THz waveguide. However, this scheme needs a large number of filaments to form the plasma cladding, e.g., about 300

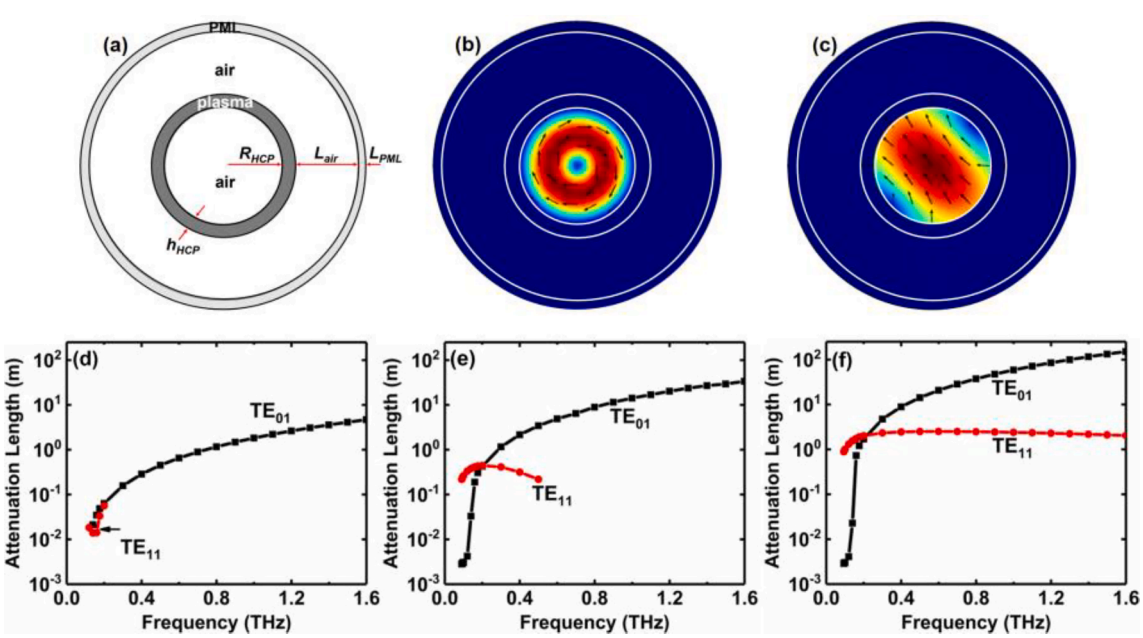

Fig. 3. (a) The simulation model set in COMSOL. The simulated transmission modes of (b) TE_{01} and (c) TE_{11}. Evolutions of attenuation lengths of TE_{01} (black squares) and TE_{11} (red circles) for (d) $N_e = 10^{15}$ cm^{-3}, (e) $N_e = 10^{17}$ cm^{-3} and (f) $N_e = 10^{19}$ cm^{-3} as a function of THz frequency.

filaments calculated for Fig. 3(a) with $R_{HCP} = 1300$ μm and $h_{HCP} = 300$ μm. In practice, thousands of filaments might be required, which is at the cost of huge laser energy (150 mJ per pulse) [25]. Remind ourselves that the spatial position of individual plasma filament in the array can be flexibly controlled, e.g., by modulating the transverse distribution of the laser energy with a phase plate, as shown in Fig. 4(a). In this case, a triangular lattice point matrix with a central point defect, i.e., a free-space photonic-crystal-like (FPC) structure is established by only 36 filaments (please see Fig. 4(b) or Fig. 1(e,f)). One will then be curious about the performance of this FPC-type waveguide in THz band. Thus in the following sections, simulations have been carried out with the verified software COMSOL and its FEM method, in order to study the transmission loss, single-mode characteristic, dispersion and band gap of this FPC structure.

3.1. The transmission mode of the FPC waveguide

Structural parameters of the FPC array are set in COMSOL including the lattice constant $\Lambda = 500$ μm and the filament diameter $d = 100$ μm, as shown in Fig. 4(b). Here the fill ratio is $d/\Lambda = 0.2$. In addition, the material parameter of a single filament was set as $N_e = 10^{17}$ cm^{-3} and the Drude-Lorentz dispersion model was selected.

Fig. 4(c) shows the simulated THz mode intensity profile (z-component of the Poynting vector) and electric field vector (black arrows) at 6 THz, which is tightly confined within the central tiny air core of the FPC structure. Note that only one of the doublet degenerated modes is illustrated here since the field is identical after a rotation of $\pi/2$ rad.

The confinement loss and attenuation length of the fundamental mode are shown in Fig. 4(d) and (e), respectively. It can be seen from Fig. 4(d) that the modal loss rapidly decreases and then tends to be stable at a relatively low value beyond 6 THz. This corresponds to Fig. 4 (e) that the attenuation length is larger in the high THz band. Moreover, one can see that the decrease of d/Λ would reduce the loss (or increase the propagation length) of the THz wave. This phenomenon could be attributed to the enhanced single-mode characteristic of the FPC structure, as shown in the following Fig. 5(a).

3.2. Endlessly single-mode characteristic of the FPC structure

As mentioned above, the decreasing THz loss inside the FPC structure is connected to the reduced d/Λ, which could be further interpreted as the enhancement of the single-mode property of the FPC structure. Briefly, when Λ increases (or d/Λ decreases), high-order modes with smaller transverse effective wavelengths are easier to leak out from the wide leakage path between two filaments. In this way, multimodes have been suppressed, and only the fundamental mode (guided mode) remains confined in the air core of the FPC structure, which is similar with the traditional PCF (photonic crystal fiber) theory of resonance tunnel [40]. Next, the single-mode characteristic of the FPC waveguide has been quantitatively investigated.

For our FPC waveguide whose cladding is the periodic arrangement of plasma filaments in air, the effective normalized frequency V_{eff} can be expressed as [40,41]:

$$V_{eff} = \frac{2\pi\Lambda}{\lambda}\sqrt{n_{co}^2 - n_{eff}^2} \tag{10}$$

where n_{co} and n_{eff} are the (effective) refractive indices of the core and guided mode, respectively. The calculated evolutions of V_{eff} at different values of d/Λ are shown in Fig. 5(a). One can see that V_{eff} becomes smaller than the critical 2.405 (horizontal line) in case of d/Λ below 0.4 (blue up-triangles), satisfying the condition of single-mode transmission in the FPC structure.

At $d/\Lambda = 0.2$, the starting point of single-mode wavelength is about lg $(\Lambda/\lambda) = 0.4$, resulting in a maximum λ of 133 μm (or minimum $f = 2.26$ THz) for endlessly single-mode THz transmission. Moreover, the growth of $\lg(\Lambda/\lambda)$ by either increasing Λ or decreasing λ will decrease V_{eff} and strengthen the single-mode property of the FPC structure.

3.3. Dispersion of the FPC structure

Due to the improved single-mode property of the FPC structure at a smaller d/Λ (Fig. 5(a)), it is expected that the THz dispersion can also be benefit from its single-mode transmission within a wide spectral range. Quantitatively, the group velocity dispersion can be evaluated by [42,43]:

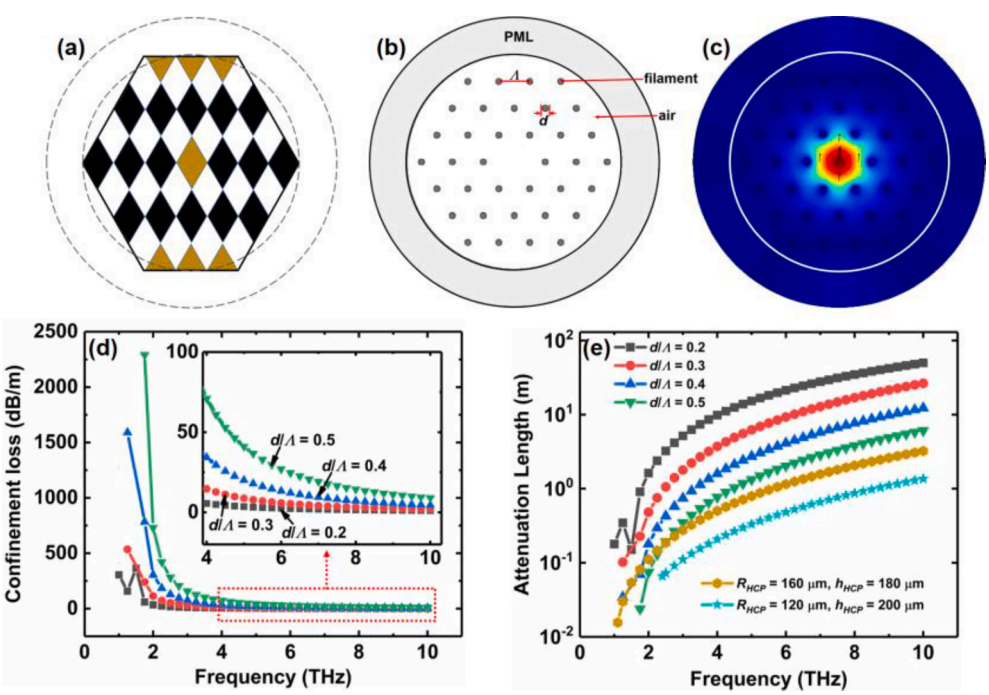

Fig. 4. (a) The phase plate designed for creating the corresponding FPC structure. It could be made of a piece of 1-mm-thick float glass with parts (in brown) opaque to the 800-nm laser, while black and white parts indicate different thicknesses induced by wet etching. This thickness difference makes a π phase lag at the laser wavelength between two adjacent parts. Thus, multi-filaments would be generated corresponding to each rhombus part of the phase plate. (b) Schematic diagram of the FPC structure ($\Lambda = 500$ μm, $d = 100$ μm, $d/\Lambda = 0.2$). (c) z-component of the Poynting vector (color) and electric vector (arrows) of one of the doublet degenerated fundamental modes at $f = 6$ THz and $N_e = 10^{17}$ cm^{-3}. (d) The confinement loss and (e) attenuation lengths of fundamental modes with respect to different d/Λ. Specifically in (e), for comparison in the attenuation length, the bottom two lines are obtained via simulations with the HCP waveguide whose plasma cladding is assumed to be built by 36 filaments.

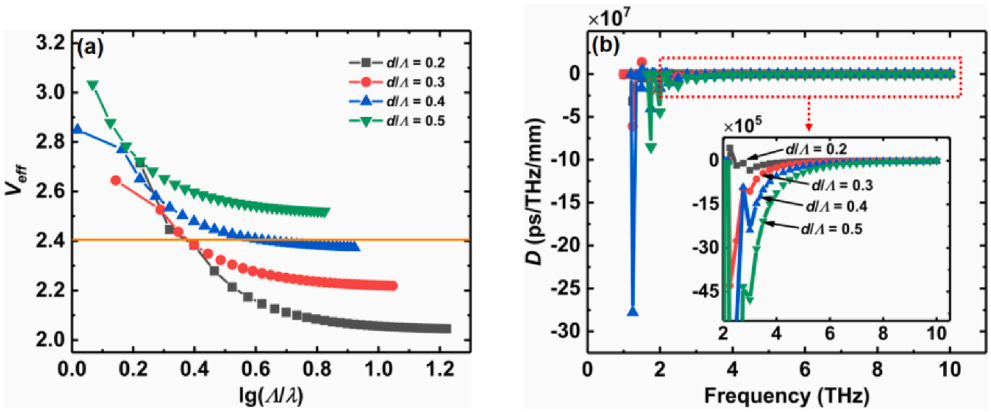

Fig. 5. (a) Effective normalized frequency V_{eff} at different d/Λ. (b) Variations of the dispersion D with respect to the THz frequency for different d/Λ.

$$D = \frac{\partial^2 h}{\partial \omega^2} \tag{11}$$

where D is the combination of the material and waveguide dispersion. Calculated results of D with different d/Λ are shown in Fig. 5(b). One can see that the overall tendency of D variation is decreasing towards high THz frequency, especially at a smaller d/Λ, which is similar with d/Λ -associated single-mode characteristic as shown in Fig. 5(a). Furthermore, strong fluctuations of D appear at the low THz band, which might be due to no stable single mode existing before $f = 2.26$ THz ($\lg(\Lambda/\lambda) = 0.4$) as predicted by Fig. 5(a).

3.4. Band gap of the FPC structure

Next, band characteristics of the fundamental and cladding modes inside the FPC structure have been roughly researched by dispersion relationships as displayed in Fig. 6(a,b). Here, d/Λ is fixed at 0.2.

It can be seen in Fig. 6(a) that both dispersion curves of the studied modes are located on the left side of the light line, i.e., the effective refractive index n_{eff} of both modes are slightly smaller than the unity, which can also be observed in Fig. 6(b). In addition, n_{eff} of the cladding mode is further smaller than that of the fundamental one as shown in Fig. 6(b). These phenomena could be due to the fact that the FPC cladding is made of plasma filament array whose refractive index n_p is below 1 (Fig. 1(g)). Thus the resulted modal indices appear as $n_{eff\text{-}cladding} < n_{eff\text{-}fundamental} < 1$.

Moreover, when n_p decreases with the increasing λ, $n_{eff\text{-}cladding}$ and $n_{eff\text{-}fundamental}$ decrease as well, as shown in Fig. 6(b). In the same figure while λ increases, the band gap between dispersion curves of the fundamental and cladding modes becomes wider because the difference between $n_{eff\text{-}cladding}$ and $n_{eff\text{-}fundamental}$ is enhanced. It can also be seen in Fig. 6(b) that the dispersion curve of the cladding mode has a certain width, as shown as the gray area, because of the strong degeneracy of cladding modes at a given λ/Λ (red circles). Besides, the photonic crystal light-cone area represents all possible extended modes in the cladding.

3.5. Comparison between HCP and FPC structures on the attenuation length

By studying THz transmission effects via the FPC structure above, one of its most impressive advantages is the spatial confinement of the THz mode field with only 36 filaments, which is quite laser-energy saving compared with the HCP scheme. However, one will still be interested in outcomes of the HCP waveguide on THz wave guiding if the same number of plasma filaments were used as the FPC case.

This time, the transverse area of the HCP ring-cladding has been set to be equal to the sum of 36 filaments (single diameter is 100 μm). Remind of ourselves that the width of the cladding h_{HCP} should be larger than the corresponding skin depth δ (~177 μm for 0.1 ~ 10 THz at $N_e = 10^{17}$ cm^{-3}). Therefore, two sets of parameters are used for HPC, i.e., $R_{HCP} = 160$ μm and $h_{HCP} = 180$ μm; $R_{HCP} = 120$ μm and $h_{HCP} = 200$ μm. The COMSOL-simulated results are shown as the bottom two lines in Fig. 4(e), from which one can see that the attenuation lengths of TE_{01} mode as for the current HCP waveguide are much shorter than that of the FPC method. This further proves the superiority of the FPC structure for THz wave guidance.

4. Discussion

In the future, several procedures should be on the schedule. Firstly, great affords still should be made on the optimization of the FPC structure, in order to further reduce the confinement loss and enhance

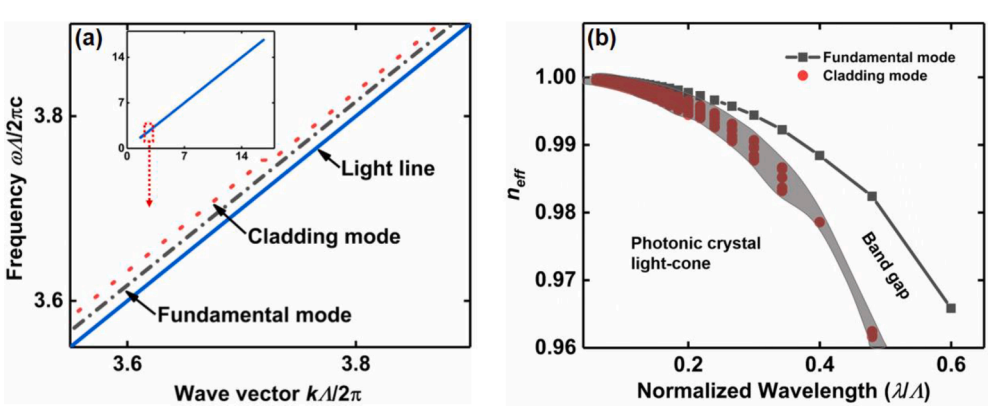

Fig. 6. (a) Band diagram of THz modes at $d/\Lambda = 0.2$. (b) Effective refractive index n_{eff} as a function of the normalized THz wavelength (λ/Λ).

the transmission distance of THz waves. Secondly, the design of phase plates (or lens array) and numerical simulations of the following laser filamentation process [23] are necessary before the final experimental demonstration of the FPC waveguide's validity. What's more, structures other than HCP or FPC, e.g., a negative curved waveguide, might also be benefited from being formed by the plasma filament array. These works have been planned and are underway.

Specifically, our experimental design is shown in Fig. 7(a). It can be seen that, in the conventional femtosecond laser filamentation setup [15], an additional phase plate is inserted in the 800-nm laser path, and the laser beam is then focused and creates a plasma filament array in air. Next, THz waves can be injected into this FPC waveguide by combinations of a side THz source (e.g., a PCA emitter), a THz lens (e.g., TPX) and an ITO plate (for reflecting THz wave). Note that a THz source with broader bandwidth can better validate our FPC structure.

Here, a delay line was used for the pumping laser beam in order to realize its temporal synchronization with the guided THz pulses. In this case, it should be emphasized that the nanosecond-scale lifetime of the laser-induced free electron (rather than the laser pulse itself) is essential for guiding the THz pulse whose duration is several picoseconds.

Remind ourselves that the plasma filament itself can also radiate THz waves. However, the laser-THz conversion efficiency is extremely low (about 10^{-11}) [44], which might be neglectable in the output THz signal after the FPC waveguide. Furthermore, one can distinguish the filament-induced THz signal from the injected one by their different characteristics, such as polarization or spectral peak frequency.

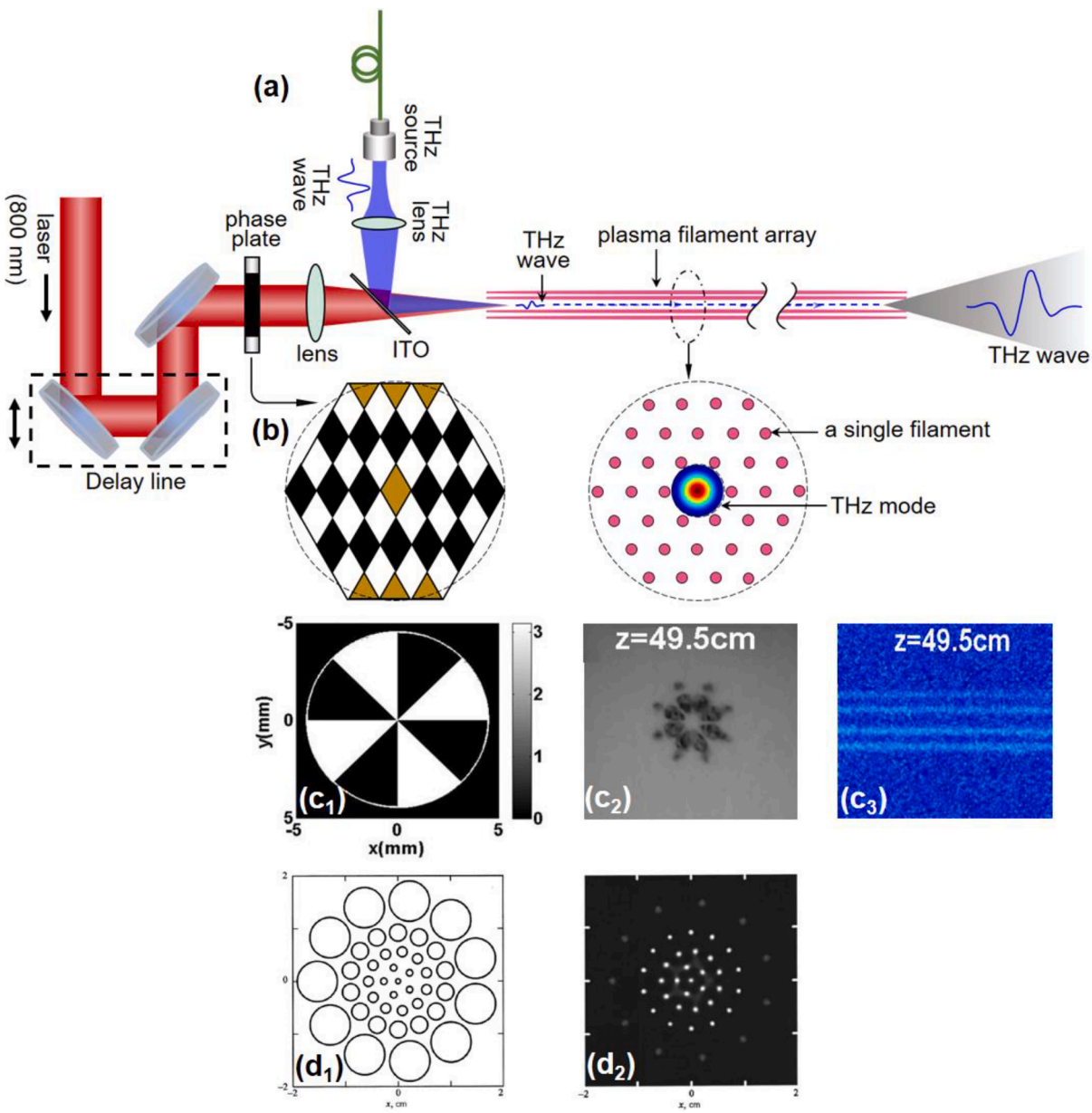

Fig. 7. (a) The designed experimental setup for testing THz guidance by the FPC structure. (b) The proposed phase plate pattern in this work, and the generated FPC structure, as well as the confined THz mode, reproduced from Fig. 4(a-c). (c_1) The reported phase plate with eight parts marked in black and white alternately. Each part and the adjacent one have a thickness difference which could make a π phase lag at the input laser wavelength (e.g., 800 nm). Multi-filaments would be generated corresponding to each part of the phase plate. (c_2) The cross-sectional distribution of the created filament array (ablation spots of the laser plasma on the thermal paper). (c_3) The corresponding side image of (c_2) (four filaments were hidden behind the observed ones). ([Reprinted/Adapted] with permission from [23] © The Optical Society). (d_1) The reported lens array and (d_2) the transverse view of the generated filament array. ([Reprinted/Adapted] with permission from [24] © The Optical Society).

The proposed phase plate, the corresponding FPC structure, and the predicted THz mode, are displayed in Fig. 7(b), which have been described in detail in Section 3. Here, it is worth mentioning that, our phase plate pattern is inspired by the reported one as shown in Fig. 7(c_1) [23], which successfully built a 8-filament array in air in the experiment (Fig. 7($c_{2\text{-}3}$)). One may also prefer another scheme of multi-lens array for generating a much more complex filament array structure as shown in Fig. 7($d_{1\text{-}2}$) [24]. Both designs in the literature could produce a stable plasma filament array with regular transverse distribution under the condition of atmospheric turbulence. If further assisted by an axicon, the longitudinal filament length could be significantly increased [23].

5. Conclusion

In summary, the guidance of THz wave inside two types of plasma waveguides, namely HCP and FPC, has been theoretically studied in this work. Analytical and numerical methods have revealed that, both waveguide structures could support THz transmission modes inside their tiny central air cores for an attenuation length up to hundreds of meters. Specifically, inside the HCP waveguide, TE_{01} mode is superior to the fundamental one of TE_{11}. While, as for the FPC structure, it is preferable to the HCP scheme for the less energy consuming of the pumping laser. Furthermore, the FPC mode with optimized parameters (such as filling ratio of the plasma to the air cladding) has a smaller mode field diameter, longer attenuation length, and better single-mode property. Compared with traditional THz waveguides such as photonic crystal fibers or anti-resonant reflection hollow pipes, the proposed plasma waveguides could find applications in case of long-distance wireless communication or atmospheric remote sensing of THz wave in a desired direction.

CRediT authorship contribution statement

Lie-Zhi Tang: . **Jia-Yu Zhao:** Conceptualization, Methodology, Supervision. **Zhang-Hua Dong:** . **Zhong-Hui Liu:** . **Wen-Ting Xiong:** . **Yu-Chen Hui:** . **Shkurinov Alexander:** . **Yan Peng:** Project administration. **Yi-Ming Zhu:** Project administration, Resources.

Declaration of Competing Interest

The authors declare that they have no known competing financial interests or personal relationships that could have appeared to influence the work reported in this paper.

Acknowledgement

Fruitful discussions with Dr. Wei Lin in Nankai University and Dr. Hui Gao in Tiangong University are appreciated.

Funding

This work was supported by Shanghai Chenguang Project (18CG53), National Natural Science Foundation of China (61722111, 11704252, 61771314, 61922059), 111 Project (D18014), International Joint Lab Program supported by Science and Technology Commission Shanghai Municipality (17590750300), Key project supported by Science and Technology Commission Shanghai Municipality (YDZX201931000049 60).

References

[1] T. Nakagawa, Observations of the Universe in the Terahertz Range: From AKARI to SPICA, IEEE T. THz Sci. Techn. 5 (6) (2015) 1133–1139.
[2] P.H. Siegel, THz Instruments for Space, IEEE T. Antenn. Propag. 55 (11) (2007) 2957–2965, https://doi.org/10.1109/TAP.2007.908557.
[3] T. Kleine-Ostmann, T. Nagatsuma, A Review on Terahertz Communications Research, J. Infrared Millim. Te. 32 (2) (2011) 143–171, https://doi.org/10.1007/s10762-010-9758-1.
[4] T. Nagatsuma, S. Horiguchi, Y. Minamikata, Y. Yoshimizu, S. Hisatake, S. Kuwano, N. Yoshimoto, J. Terada, H. Takahashi, Terahertz wireless communications based on photonics technologies, Opt. Exp. 21 (20) (2013) 23736–23747, https://doi.org/10.1364/OE.21.023736.
[5] F.C.D. Lucia, D.T. Petkie, H.O. Everitt, A Double Resonance Approach to Submillimeter/Terahertz Remote Sensing at Atmospheric Pressure, IEEE J. Quantum Elect. 45 (2) (2009) 163–170, https://doi.org/10.1109/JQE.2008.912473.
[6] G.S. Nusinovich, D.G. Kashyn, Y. Tatematsu, T. Idehara, Effect of atmospheric conditions on operation of terahertz systems for remote detection of ionizing materials, Phys. Plasmas 21 (1) (2014) 013108, https://doi.org/10.1063/1.4862779.
[7] G.-R. Kim, T.-I. Jeon, D. Grischkowsky, 910-m propagation of THz ps pulses through the Atmosphere, Opt. Exp. 25 (21) (2017) 25422–25434, https://doi.org/10.1364/OE.25.025422.
[8] G.-R. Kim, K. Moon, K.H. Park, J.F. O'Hara, D. Grischkowsky, T.-I. Jeon, Remote N_2O gas sensing by enhanced 910-m propagation of THz pulses, Opt. Exp. 27 (20/30) (2019) 27514–27522, https://doi.org/10.1364/OE.27.027514.
[9] G. Gallot, S.P. Jamison, R.W. McGowan, D. Grischkowsky, Terahertz waveguides, J. Opt. Soc. Am. B 17 (5) (2000) 851–863, https://doi.org/10.1364/JOSAB.17.000851.
[10] R. Mendis, D. Grischkowsky, Undistorted guided-wave propagation of subpicosecond terahertz pulses, Opt. Lett. 26 (11) (2001) 846–848, https://doi.org/10.1364/OL.26.000846.
[11] R. Mendis, D. Grischkowsky, THz interconnect with low-loss and low-group velocity dispersion, IEEE Microwave Wireless Comp. Lett. 11 (11) (2001) 444–446, https://doi.org/10.1109/7260.966036.
[12] D. Chen, H. Chen, A novel low-loss Terahertz waveguide: Polymer tube, Opt. Exp. 18 (4) (2010) 3762–3767, https://doi.org/10.1364/OE.18.003762.
[13] K. Wang, D.M. Mittleman, Metal wires for terahertz wave guiding, Nature 432 (7015) (2004) 376–379, https://doi.org/10.1038/nature03040.
[14] H. Han, H. Park, M. Cho, J. Kim, Terahertz pulse propagation in a plastic photonic crystal fiber, Appl. Phys. Lett. 80 (15) (2002) 2634–2636, https://doi.org/10.1063/1.1468897.
[15] J. Zhao, Y. Zhang, Z. Wang, W. Chu, B. Zeng, W. Liu, Y.a. Cheng, Z. Xu, Propagation of terahertz wave inside femtosecond laser filament in air, Laser Phys. Lett. 11 (9) (2014) 095302, https://doi.org/10.1088/1612-2011/11/9/095302.
[16] A. Couairon, A. Mysyrowicz, Femtosecond filamentation in transparent media, Phys. Rep. 441 (2–4) (2007) 47–189, https://doi.org/10.1016/j.physrep.2006.12.005.
[17] B. La Fontaine, F. Vidal, Z. Jiang, C.Y. Chien, D. Comtois, A. Desparois, T. W. Johnston, J.-C. Kieffer, H. Pépin, H.P. Mercure, Filamentation of ultrashort pulse laser beams resulting from their propagation over long distances in air, Phys. Plasmas 6 (5) (1999) 1615–1621, https://doi.org/10.1063/1.873715.
[18] M. Rodriguez, R. Bourayou, G. Méjean, J. Kasparian, J. Yu, E. Salmon, A. Scholz, B. Stecklum, J. Eislöffel, U. Laux, A.P. Hatzes, R. Sauerbrey, L. Wöste, J.-P. Wolf, Kilometer-range nonlinear propagation of femtosecond laser pulses, Phys. Rev. E 69 (3) (2004), https://doi.org/10.1103/PhysRevE.69.036607.
[19] M. Alshershby, Z. Hao, J. Lin, Guiding microwave radiation using laser-induced filaments: the hollow conducting waveguide concept, J. Phys. D: Appl. Phys. 45 (26) (2012) 265401, https://doi.org/10.1088/0022-3727/45/26/265401.
[20] M. Alshershby, Z. Hao, J. Lin, Analysis of microwave leaky modes propagating through laser plasma filaments column waveguide, Phys. Plasmas 19 (12) (2012) 123504, https://doi.org/10.1063/1.4771595.
[21] M. Alshershby, Z.Q. Hao, A. Camino, J.Q. Lin, Modeling a femtosecond filament array waveguide for guiding pulsed infrared laser radiation, Opt. Commun. 296 (2013) 87–94, https://doi.org/10.1016/j.optcom.2012.12.067.
[22] N. Jhajj, E.W. Rosenthal, R. Birnbaum, J.K. Wahlstrand, H.M. Milchberg, Demonstration of long-lived high-power optical waveguides in air, Phys. Rev. X 4 (1) (2014), 011027, https://doi.org/10.1364/CLEO_SI.2014.STh1E.3.
[23] H. Gao, W. Chu, G.L. Yu, B. Zeng, J.Y. Zhao, Z. Wang, W.W. Liu, Y. Cheng, Z.Z. Xu, Femtosecond laser filament array generated with step phase plate in air, Opt. Exp. 21 (4) (2013) 4612–4622, https://doi.org/10.1364/OE.21.004612.
[24] N.A. Panov, O.G. Kosareva, I.N. Murtazin, Ordered filaments of a femtosecond pulse in the volume of a transparent medium, J. Opt. Technol. 73 (11) (2006) 778–785, https://doi.org/10.1364/JOT.73.000778.
[25] M. Châteauneuf, S. Payeur, J. Dubois, J.-C. Kieffer, Microwave guiding in air by a cylindrical filament array waveguide, Appl. Phys. Lett. 92 (9) (2008) 091104, https://doi.org/10.1063/1.2889501.
[26] V.P. Kandidov, A.E. Dormidonov, O.G. Kosareva, N. Akozbek, M. Scalora, S. L. Chin, Optimum small-scale management of random beam perturbations in a femtosecond laser pulse, Appl. Phys. B 87 (1) (2007) 29–36, https://doi.org/10.1007/s00340-006-2555-9.
[27] J. Zhao, W. Chu, Z. Wang, Y. Peng, C. Gong, L. Lin, Y. Zhu, W. Liu, Y.a. Cheng, S. Zhuang, Z. Xu, Strong Spatial Confinement of Terahertz Wave inside Femtosecond Laser Filament, ACS Photonics 3 (12) (2016) 2338–2343, https://doi.org/10.1021/acsphotonics.6b00512.
[28] V.L. Ginzburg, W.L. Sadowski, D.M. Gallik, S.C. Brown, Propagation of electromagnetic waves in plasma, Phys. Today 15 (10) (1962) 70–73, https://doi.org/10.1063/1.3057811.
[29] A. Houard, Y. Liu, B. Prade, V.T. Tikhonchuk, A. Mysyrowicz, Strong Enhancement of Terahertz Radiation from Laser Filaments in Air by a Static Electric Field, Phys.

Rev. Lett. 100 (25) (2008), 255006, https://doi.org/10.1103/PhysRevLett.100.255006.
[30] H. Yang, J. Zhang, Y. Li, J. Zhang, Y. Li, Z. Chen, H. Teng, Z. Wei, Z. Sheng, Characteristics of self-guided laser plasma channels generated by femtosecond laser pulses in air, Phys. Rev. E 66 (1) (2002), 016406, https://doi.org/10.1103/PhysRevE.66.016406.
[31] A. Camerlingo, X. Feng, F. Poletti, G.M. Ponzo, F. Parmigiani, P. Horak, M. N. Petrovich, P. Petropoulos, W.H. Loh, D.J. Richardson, Near-zero dispersion, highly nonlinear lead-silicate W-type fiber for applications at 1.55μm, Opt. Exp. 18 (15) (2010) 15747–15756, https://doi.org/10.1364/OE.18.015747.
[32] S. Kawakami, S. Nishida, Perturbation theory of a doubly clad optical fiber with a low-index inner cladding, IEEE J. Quant. Elect. 11 (4) (1975) 130–138, https://doi.org/10.1109/JQE.1975.1068578.
[33] B.H. Shaw, S. Steinke, J. van Tilborg, W.P. Leemans, Reflectance characterization of tape-based plasma mirrors, Phys. Plasmas 23 (6) (2016) 063118, https://doi.org/10.1063/1.4954242.
[34] V.V. Valuev, A.E. Dormidonov, V.P. Kandidov, S.A. Shlenov, V.N. Kornienko, V. A. Cherepenin, Plasma channels formed by a set of filaments as a guiding system for microwave radiation, J. Commun. Technol. Elect. 55 (2) (2010) 208–214, https://doi.org/10.1134/S1064226910020130.
[35] V.D. Zvorykin, A.O. Levchenko, A.V. Shutov, E.V. Solomina, N.N. Ustinovskii, I. V. Smetanin, Long-distance directed transfer of microwaves in tubular sliding-mode plasma waveguides produced by KrF laser in atmospheric air, Phys. Plasmas 19 (3) (2012) 033509, https://doi.org/10.1063/1.3692090.
[36] M. Navarro-Cia, C.M. Bledt, J.E. Melzer, M.S. Vitiello, H.E. Beere, D.A. Ritchie, J. A. Harrington, O. Mitrofanov, Dispersion and attenuation in flexible dielectric-lined hollow metallic THz waveguides", IRMMW-THz IEEE (2013) https://doi.org/10.1109/IRMMW-THz.2013.6665718.
[37] B. Bowden, J.A. Harrington, O. Mitrofanov, Low-loss modes in hollow metallic terahertz waveguides with dielectric coatings, Appl. Phys. Lett. 93 (18) (2008) 181104, https://doi.org/10.1063/1.3013585.
[38] M. Ibanescu, S.G. Johnson, M. Soljačić, J.D. Joannopoulos, Y. Fink, O. Weisberg, T. D. Engeness, S.A. Jacobs, M. Skorobogatiy, Analysis of mode structure in hollow dielectric waveguide fibers, Phys. Rev. E 67 (4) (2003), 046608, https://doi.org/10.1103/PhysRevE.67.046608.
[39] M. Navarro-Cia, C.M. Bledt, M.S. Vitiello, H.E. Beere, D.A. Ritchie, J.A. Harrington, O. Mitrofanov, Modes in silver-iodide-lined hollow metallic waveguides mapped by terahertz near-field time-domain microscopy, J. Opt. Soc. Am. B 30 (1) (2013) 127–135, https://doi.org/10.1364/JOSAB.30.000127.
[40] T.A. Birks, J.C. Knight, P.St.J. Russell, Endlessly single-mode photonic crystal fiber, Opt. Lett. 22 (13) (1997) 961–963, https://doi.org/10.1364/OL.22.000961.
[41] K. Nielsen, H.K. Rasmussen, P.U. Jepsen, O. Bang, Porous-core honeycomb bandgap THz fiber, Opt. Lett. 36 (5) (2011) 666–668, https://doi.org/10.1364/OL.36.000666.
[42] Haisu Li, Mei Xian Low, Rajour Tanyi Ako, Madhu Bhaskaran, Sharath Sriram, Withawat Withayachumnankul, Boris T. Kuhlmey, Shaghik Atakaramians, Broadband Single-Mode Hybrid Photonic Crystal Waveguides for Terahertz Integration on a Chip, Adv. Mater. Technol. 5 (7) (2020) 2000117, https://doi.org/10.1002/admt.v5.710.1002/admt.202000117.
[43] H. Bao, K. Nielsen, O. Bang, P.U. Jepsen, Dielectric tube waveguides with absorptive cladding for broadband, low-dispersion and low loss THz guiding, Sci. Rep. 5 (2015) 7620, https://doi.org/10.1038/srep07620.
[44] C.D. Amico, A. Houard, S. Akturk, Y. Liu, J. Le Bloas, M. Franco, B. Prade, A. Couairon, V.T. Tikhonchuk, A. Mysyrowicz, Forward THz radiation emission by femtosecond filamentation in gases: theory and experiment, New J. Phys. 10 (1) (2008) 013015, https://doi.org/10.1088/1367-2630/10/1/013015.